The phase separation due to A-site-cation size mismatch in $La_{0.5}Ca_{0.5-x}Ba_xMnO_3$

2001 J. Phys.: Condens. Matter 13 1627

(http://iopscience.iop.org/0953-8984/13/8/302)

INSTITUTE OF PHYSICS PUBLISHING JOURNAL OF PHYSICS: CONDENSED MATTER

J. Phys.: Condens. Matter **13** (2001) 1627–1639 www.iop.org/Journals/cm PII: S0953-8984(01)15574-8

The phase separation due to A-site-cation size mismatch in $La_{0.5}Ca_{0.5-x}Ba_xMnO_3$

Hironori Wakai

Department of Mechanical Engineering and Materials Science, Faculty of Engineering, Yokohama National University, Tokiwadai, Hodogaya-ku, Yokohama 240-8501, Japan

E-mail: d00ja012@ynu.ac.jp

Received 14 July 2000

Abstract

The relationship between electronic and magnetic properties and the lattice effect due to replacement of A-site cations with size mismatch has been studied in the $La_{0.5}Ca_{0.5-x}Ba_xMnO_3$ system with the amount of Mn^{4+} fixed at 0.48. Three sorts of compound ($x = 0$, 0.1 and 0.2) have been prepared, and resistivity, magnetic susceptibility, thermopower and x-ray photoelectron spectroscopy (XPS) measurements were carried out. Every compound exhibits the metal–insulator transition at T_{MI} and a ferromagnetic–paramagnetic phase transition at T_c, which is different from T_{MI}. Decrease of T_c and increase of the magnetic susceptibility below T_c with increasing x, and complex behaviour of the resistivity are observed. It is possible to explain these results on the basis of the assumption of a phase separation into ferromagnetic metal and insulator phases. The XPS measurement result indicates that in the $x = 0.2$ compound, the insulator phase exists at the temperature at which ferromagnetism is observed. I find that a good fit of the thermopower data for the $x = 0.2$ compound is obtained by taking into account contributions of both ferromagnetic metal and insulator phases at $T < T_c$. It is suggested that the lattice effect with large values of not only t but also σ^2 promotes the phase separation into ferromagnetic metal and Jahn–Teller insulator phases at $T < T_c$.

1. Introduction

The mixed-valence perovskite manganites $La_{1-x}A_xMnO_3$ (A = Ca, Sr and Ba) have been investigated for many years due to their interesting magnetic and transport properties, especially the colossal-magnetoresistance (CMR) effect [1–3]. As is well known, the parent compound $LaMnO_3$ shows basically an antiferromagnetic (AFM) insulator behaviour. Upon deviation of the oxygen stoichiometry and by substituting a divalent cation (A^{2+}), such as Ca^{2+}, Sr^{2+} or Ba^{2+}, in place of La^{3+}, $La_{1-x}A_xMnO_3$ exhibits a ferromagnetic (FM) ground state; meanwhile, a metal–insulator transition occurs near the magnetic transition temperature T_c.

0953-8984/01/081627+13$30.00

These phenomena have been traditionally explained with double-exchange (DE) theory based on the exchange of electrons between Mn^{3+} and Mn^{4+} ions [4]. However, it is suggested that DE alone is not sufficient to explain all of the physics of these mixed-valence compounds. The importance of lattice distortion due to strong electron–phonon coupling in addition to DE has been stressed and discussed intensively [5, 6]. This electron–phonon coupling is due to the fact that the Mn^{3+} ion is of Jahn–Teller (JT) type. Localization of the charge carriers with JT distortion is very likely to be a key factor in discussion of the physical properties.

Furthermore, the lattice distortion created by replacing A-site cations with various ions has attracted strong interest [7–9]. This substitution mainly causes a distortion of the Mn–O–Mn bond angle which influences the transfer of e_g electrons between Mn sites. Hwang *et al* have investigated (La, Pr, Y)$_{0.7}$Ca$_{0.3}$MnO$_3$ with fixed carrier concentration, and found that with reduction of $\langle r_A \rangle$, which represents the average ionic radius of A-site cations, T_c and the conductivity decrease [9]. It is suggested that the principal effect of decreasing $\langle r_A \rangle$ is that of decreasing the Mn–O–Mn bond angle, thereby weakening the DE and reducing the transfer of e_g electrons between Mn^{3+} and Mn^{4+}.

Recently, Rodriguez-Martinez and Attfield suggested that the electronic and magnetic properties depend sensitively not only on $\langle r_A \rangle$ but also on the variance (second moment) σ^2. They have found that as σ^2 increases, local deformations of Mn–O$_6$ octahedra are induced and T_c decreases for a constant $\langle r_A \rangle$ value [10]. The lattice effect of σ^2 has been studied in series such as $R^{3+}_{0.7}A^{2+}_{0.3}MnO_3$ (R = La, Pr, Nd, Sm; A = Ca, Sr, Ba) with constant $\langle r_A \rangle = 1.23$ Å [10], Th$_{0.35}$(Ba, Sr, Ca)$_{0.65}$MnO$_3$ with constant $\langle r_A \rangle = 1.255$ Å [11] and (La, Dy)$_{0.7}$Ca$_{0.3}$MnO$_3$ [12] in which La^{3+} is replaced by the smaller Dy^{3+}.

In almost all of the reports, the lattice effects have been investigated by the means of the replacement of A-site cations giving σ^2 various values with constant $\langle r_A \rangle$ and the substitution increasing σ^2 with reduction of $\langle r_A \rangle$ in manganites which have the ferromagnetic metal (FMM) ground state below T_c. Each decrease of $\langle r_A \rangle$ and increase of σ^2 suppresses the transfer of e_g electrons between Mn sites. However, the lattice effect when the A-site cation is replaced by a larger ion in the FMM ground state is not yet clear. Therefore, the lattice effect caused by the replacement of an A-site cation with a larger ion, which increases σ^2 with $\langle r_A \rangle$, is still under investigation. Moreover, it is suggested that the local deformations of the Mn–O$_6$ octahedra due to the A-site-cation disorder and size effect act as 'preformed JT distortions' which promote the localization of e_g electrons [10]. Hence, there is a possibility that an electrical phase separation into the FMM and JT insulator phases is caused by the local lattice distortion with a large value of σ^2. Recently, the electrical phase separation has attracted strong interest [13–16]; it is important to study the correlation between the phase separation and the local lattice distortion.

In view of these points, I substituted Ba^{2+} for Ca^{2+} in La$_{0.5}$Ca$_{0.5}$MnO$_3$, fixing the Mn^{4+} fraction. The reason for choosing La$_{0.5}$Ca$_{0.5}$MnO$_3$ as a starting material is that the electronic and transport properties of this compound are expected to be very sensitive to the lattice effect because La$_{0.5}$Ca$_{0.5}$MnO$_3$ is under the FMM–AFM insulator phase boundary [17]. The present study has employed measurements of the electrical resistivity, magnetic susceptibility and thermopower, and x-ray photoemission spectroscopy (XPS).

2. Experimental details

Polycrystalline specimens of La$_{0.5}$Ca$_{0.5-x}$Ba$_x$MnO$_3$ ($x = 0$, 0.1 and 0.2) were prepared by the conventional solid-state reaction method. Stoichiometric proportions of La_2O_3, $CaCO_3$, $BaCO_3$ and MnO_2 powders with 99.99% purity were mixed and calcined in air at 1250 °C for 24 h and, after being ground very carefully, calcined again in air at 1300 °C for 24 h. The

powders were then pressed into pellets and finally sintered in air at 1450 °C for 48 h. The grain size of the compounds was found to be ∼7 μm by scanning electron microscope studies.

The chemical analyses by the wet process yielded the chemical compositions, and the oxygen contents were determined by redox titration. I determined the Mn^{4+} fraction to be ±1% Mn^{4+} for each compound. As shown in table 1, the Mn^{4+} fractions in every compound are equal within the experimental errors. The mean valence of Mn is $Mn^{3.48+}$. Powder x-ray diffraction measurements were made for all compounds, and the diffraction patterns obtained indicate that every compound has orthorhombic perovskite structure without any other secondary or impurity phases. As shown in table 1, the lattice constants, a, b and c, at room temperature increase with Ba doping.

Table 1. Lattice parameters (a, b and c) at room temperature, Mn^{4+} fractions ([Mn^{4+}]) and the ratios of the oxygen content to the manganese content ([O]/[Mn]) for $La_{0.5}Ca_{0.5-x}Ba_xMnO_3$ compounds.

x	a (Å)	b (Å)	c (Å)	[Mn^{4+}]	[O]/[Mn]
0	5.441	7.655	5.429	0.477	3.03
0.1	5.473	7.675	5.446	0.480	3.03
0.2	5.494	7.711	5.469	0.480	3.02

The dc resistivity measurements were performed by the standard four-probe method, using a Keithley 619 resistance bridge and an Advantest TR 6871 digital multimeter with an Advantest R 6161 power supply. The magnetic susceptibilities (χ) were measured by using a Quantum Design superconducting interference device magnetometer (SQUID) with an applied field of 0.01 T at temperatures in the range 10–330 K. Thermopower (Seebeck coefficient) measurements were carried out between 80 and 310 K on a sample placed between two blocks of oxygen-free high-conductivity (OFHC) copper across which a constant temperature gradient was applied. Electrical contacts were achieved with silver paste. XPS spectra were obtained at room temperature and 133 K by using a commercial x-ray photoelectron spectrometer with a monochromatized Al Kα line, at 1486.6 eV (PHI ESCA−5600). The base pressure in the chamber was about 10^{-12} atm and the cleanliness of the compound surface was checked by examining the C 1s peak at 248.6 eV. Core-level binding energies were referenced to this C 1s peak to account for the surface charging.

3. Results and discussion

For all compounds, as shown in table 1, the amounts of Mn^{4+} and the ratios of the oxygen content to the manganese content are nearly equal: [Mn^{4+}] $\cong$ 0.48 and [O]/[Mn] $\cong$ 3.03. Therefore, Ba substitution for Ca mainly changes the three-dimensional network of Mn–O_6 octahedra, and does not change the Mn valence. Hence, the correlation between the transport and magnetic properties and the lattice distortion created by the substitution can clearly be seen. Checking the Mn valence is very important in this study, because Roy *et al* report that the electronic and magnetic properties of $La_{1-y}Ca_yMnO_3$ near $y = 0.5$, which is the metal–insulator phase boundary, are very sensitive to the Mn^{4+} fraction [18].

3.1. Electronic and magnetic properties

The measured temperature dependence of the ZFC (zero-field-cooled-run) and FC (field-cooled-run) magnetic susceptibilities for all of the compounds are shown in figure 1. The applied magnetic field was 0.01 T. A transition from a low-temperature ferromagnetic phase

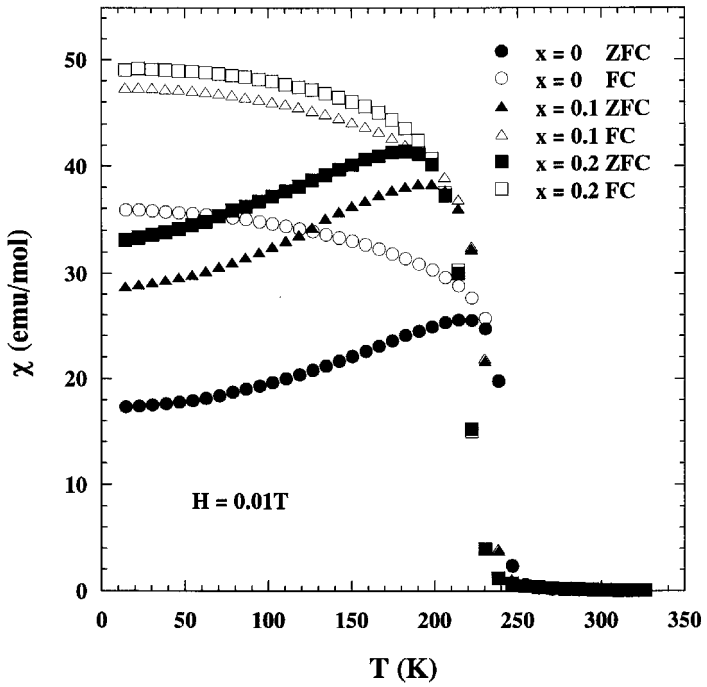

Figure 1. The temperature dependence of χ for $La_{0.5}Ca_{0.5-x}Ba_xMnO_3$ where χ is the magnetic susceptibility obtained from ZFC (solid) and FC (open) runs at 0.01 T: circles, triangles and squares for $x = 0$, 0.1 and 0.2, respectively.

to a high-temperature paramagnetic phase occurs. The magnetic transition temperature T_c is determined as the temperature at which $d\chi/dT$ is a minimum, and its values are summarized in table 2. An increase of χ below T_c and a decrease of T_c with increasing x are observed. In this work, the increase of χ at $T < T_c$ suggests that the ferromagnetic DE interaction becomes stronger with increasing x. It is noteworthy that a large difference between the ZFC and FC magnetic susceptibilities is observed below T_c for all of the compounds. This result is similar to the spin-glass behaviour observed for other compounds, such as $(La, Tb)_{2/3}Ca_{1/3}MnO_3$ [19], $(La, Dy)_{0.7}Ca_{0.3}MnO_3$ [12] and $La_{0.7}Pb_{0.3}(Mn, Fe)O_3$ [20]. Spin-glass states arise due to a strong competition between the ferromagnetic DE interaction and the antiferromagnetic superexchange interaction, which prevents the occurrence of long-range magnetic order. Therefore, it is considered that there is a competition between the FM and AFM interactions at $T < T_c$.

Table 2. Tolerance factors (t), variances of the A-site-cation size mismatch (σ^2), magnetic transition temperatures (T_c), metal–insulator transition temperatures (T_{MI}) and the activation energies required for electronic conduction in the paramagnetic insulator region above T_c (E_{hop}) for $La_{0.5}Ca_{0.5-x}Ba_xMnO_3$.

x	T_c (K)	T_{MI} (K)	t	σ^2 (Å^2)	E_{hop} (meV)
0	242	211	0.9245	0.0003	130
0.1	232	181	0.9348	0.0068	113
0.2	220	135	0.9451	0.0117	106

In figure 2, the temperature dependence of the resistivity is shown. The metal–insulator transition temperature T_{MI} is obtained as the temperature where ρ is maximum, and its values are summarized in table 2. T_{MI} lowers with increasing Ba doping. It is noticed that T_c is not the same as T_{MI}, and the discrepancy between T_c and T_{MI} increases with increasing x. All of the compounds show the metallic behaviour, $d\rho/dT > 0$, below T_{MI} and insulating behaviour, $d\rho/dT < 0$, above T_{MI}. It is worth noting that FM insulator behaviour is observed at $T_{MI} < T < T_c$. The ρ–T curves have a shoulder at T_c, and this result indicates that the transport properties should change at this temperature.

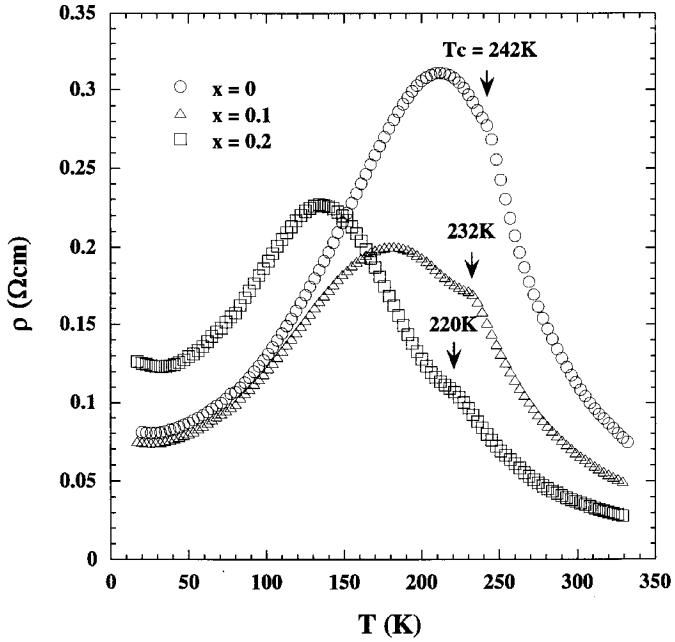

Figure 2. The temperature dependence of the resistivity for $La_{0.5}Ca_{0.5-x}Ba_xMnO_3$: open circles for $x = 0$, triangles for $x = 0.1$ and squares for $x = 0.2$. The arrows show the magnetic transition points (T_c) determined from magnetic susceptibility measurement.

In this system, the lattice distortion is created in the three-dimensional network of Mn–O_6 octahedra by replacement of Ca^{2+} with Ba^{2+}. Because Ba^{2+} has a larger ionic radius than Ca^{2+}, the Mn–O–Mn bond angle increases toward 180° with x. This is explained by the tolerance factor t, defined as

$$t = \frac{\langle r_A \rangle + r_O}{\sqrt{2}(r_{Mn} + r_O)} \tag{1}$$

where $\langle r_A \rangle$ is the average ionic radius of A-site ions, r_O is the ionic radius of O^{2-} and r_{Mn} is the average ionic radius of Mn ions at the B site. This factor represents the microscopic distortion from the ideal cubic perovskite structure ($t = 1$). For $t = 1$, the Mn–O–Mn bond angle should be 180°. For $t < 1$, the Mn–O_6 octahedra tilt and rotate to fill the excess space around the A site; this results in a decrease of the bond angle from 180°. Table 2 includes the tolerance factor t calculated from tabulated values [21], and t increases with x. The Mn–O–Mn bond angle influences the transfer integral of e_g-electron hopping between Mn^{3+} and Mn^{4+}. Increase of the Mn–O–Mn bond angle enhances the transfer of e_g electrons between Mn sites and the DE interaction [9]. Therefore, it is considered that the FMM feature becomes stronger with

increase of x. In fact, ρ below T_{MI} decreases when x increases from 0 to 0.1 as shown in figure 2. However, increasing of Ba doping from 0.1 to 0.2 causes an unexpected upturn in the resistivity at variance with the increase of the magnetic susceptibility. The DE theory indicates that the effective charge transfer $\widetilde{t_{ij}}$ between the neighbouring Mn sites depends on the relative angle $\Delta\theta_{ij}$ of the local t_{2g} spins as $\widetilde{t_{ij}} = t_{ij}\cos(\Delta\theta_{ij}/2)$ [22]. Thus, the FM spin arrangement tends to increase the effective conduction. The behaviours of ρ and χ for x increasing from 0.1 to 0.2 imply that the tolerance factor t alone is not sufficient to explain the behaviour of the present system.

It must be noted that the tolerance factor t is a value estimated from $\langle r_A \rangle$. It should be taken into consideration that A-site-ion replacement by ions with very different radii, such as replacement of Ca^{2+} ($r_{Ca} = 1.18$ Å) by Ba^{2+} ($r_{Ba} = 1.47$ Å), makes the network of Mn–O_6 octahedra microscopically inhomogeneous. Furthermore, large local distortion is expected to occur in the three-dimensional network of Mn–O_6 octahedra because the ideal $\langle r_A \rangle$ yielding $t = 1$ is 1.41 Å, which is smaller than r_{Ba}. To quantify the size mismatch effect, Rodriguez-Martinez and Attfield have used the variance (second moment) of the distribution of the A-site-cation radii, σ^2, defined as

$$\sigma^2 = \sum y_i r_i^2 - \langle r_A \rangle^2 \tag{2}$$

where i labels the three kinds of A-site ion, r_i is the radius of each A-site ion and y_i is the fractional occupancy of ion i ($\sum y_i = 1$) [10]. It is suggested that there are large local lattice distortions around Ba ions, because A-site-cation size disorder results mainly in random displacements of oxide ions from their average crystallographic positions. The size mismatch effect with a large value of σ^2 causes a local distortion of Mn–O_6 octahedra [10, 23], which corresponds to a local and random deformation of the Mn–O–Mn bond angle; thereby it is considered that the transfer of e_g electrons between Mn sites is depressed around Ba ions. It is highly probable that the local lattice distortion tends to make e_g electrons localize, leading to the JT distortion when σ^2 is large. As tabulated in table 2, σ^2 increases with x. The decrease of T_c with increasing σ^2 observed in the present system is consistent with previous reports [10–12]. This result indicates that there is some relationship between the decrease of T_c and the local localization of e_g electrons, which prevents long-range ferromagnetic ordering, because it is hard to see how the double-exchange interaction can occur without e_g-electron hopping between Mn^{3+} and Mn^{4+}. One of the predominant reasons for ρ increasing with x from 0.1 to 0.2 is that the local lattice distortion created by the substitution is accompanied with localization of e_g electrons. However, it is impossible to explain this by considering only the σ^2-effect decrease of ρ with increasing x from 0 to 0.1 and the increasing of χ at $T < T_c$ with x.

Therefore, it is considered that two opposing effects are operative for compounds containing Ba ions below T_c. One effect enhances transfer of e_g electrons between Mn sites, and the other effect localizes e_g electrons locally. It is not unexpected that the coexistence of these two opposing effects causes a phase segregation into FMM and insulator phases below T_c, because the coexistence of FMM and charge-ordered insulator phases was found in $La_{0.5}Ca_{0.5}MnO_3$ [15, 16]. Taking the phase separation into account, I give a possible explanation for the complex resistivity behaviour. ρ below T_{MI} decreases for x increasing from 0 to 0.1 because the contribution of the insulator phase is relatively small; the effect of enhancing the FMM feature is stronger. And the unexpected upturn in the resistivity with x increasing from 0.1 to 0.2 occurs because the effective metallic path reduces due to the increase of the contribution of the insulator phase. It is considered that the FM insulator behaviour obtained between T_c and T_{MI} reflects the competition between the two phases.

In order to obtain more information on magnetic properties, $\Delta\chi = (\chi_{FC} - \chi_{ZFC})/\chi_{ZFC}$ is plotted as a function of the T/T_c for every compound, and shown in figure 3. A decrease of $\Delta\chi$ with increasing x is observed. $\Delta\chi$ reflects the spin response to the applied magnetic field because the Mn valence is not changed by Ba doping. The large value of $\Delta\chi$ implies that there is a FM component whose magnitude is determined by the strong competition between the FM and AFM interactions, and FM spin arrangement is easily enhanced by cooling in an applied field of 0.01 T. $\Delta\chi$ decreasing with increasing χ below T_c indicates that the ferromagnetic interaction is strengthened more than the antiferromagnetic one, and an AFM component which is influenced by field cooling decreases with increasing x. It is suggested that the AFM component enhanced by localization of e_g electrons, whose enhancement is promoted with increase of x, is less sensitive to an applied magnetic field such as 0.01 T. Therefore, it is considered that the presence of the insulator phase prevents long-range FM ordering in spite of the increasing of the FM component. This is one of the predominant reasons for the reduction of T_c, in contrast to the increasing of the magnetic susceptibility below T_c, when σ^2 increases.

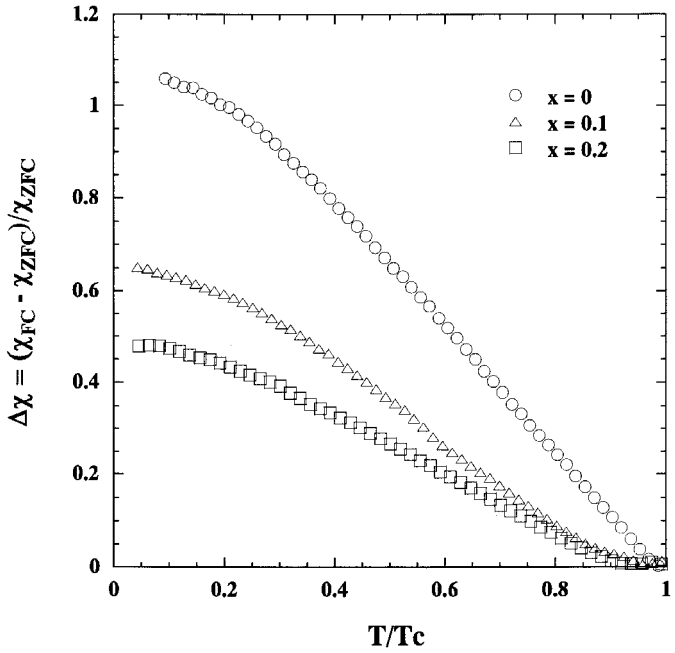

Figure 3. $\Delta\chi = (\chi_{FC} - \chi_{ZFC})/\chi_{ZFC}$ against T/T_c for $La_{0.5}Ca_{0.5-x}Ba_xMnO_3$: open circles for $x = 0$, triangles for $x = 0.1$ and squares for $x = 0.2$. χ_{ZFC} and χ_{FC} are the ZFC and FC magnetic susceptibilities, respectively.

Figure 4 displays the measured temperature dependence of the thermopower (Seebeck coefficient) for every compound, and large differences between compounds are not observed, although there is a slight variation below 150 K. The Seebeck coefficient S is independent of temperature at $T > T_c$, and this result suggests that the carrier concentration is nearly constant above T_c. Such a behaviour is very similar to that obtained for $La_{0.55}Ca_{0.45}MnO_3$ [24]. I assume, in accordance with current thought, that the conductivity in the paramagnetic regime could be described using the Emin–Holstein theory of the adiabatic small-polaron model [25]. In the temperature regime above T_c, the temperature dependences of ρ and S are described, respectively, by $\rho(T) = \rho_0 T \exp(E_{hop}/k_B T)$ and $S(T) = (k_B/e)(E_S/k_B T + \alpha)$, where k_B

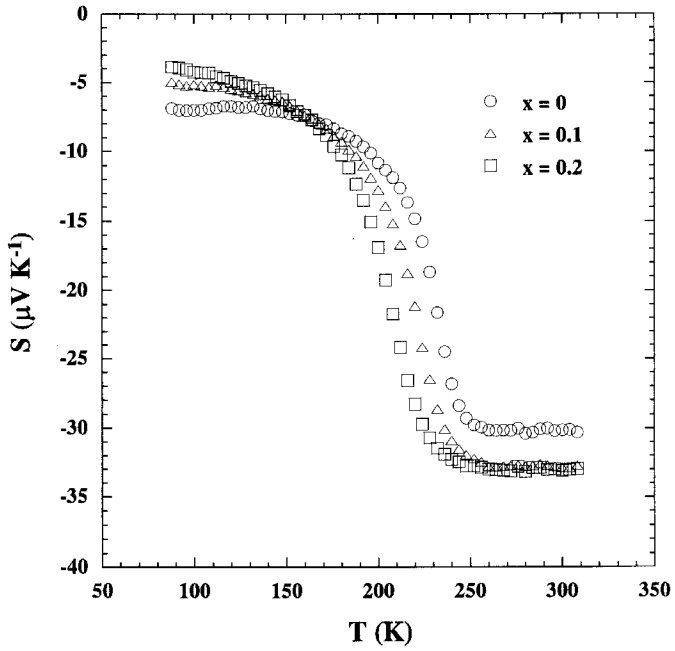

Figure 4. S (thermopower) versus T plotted for every compound: open circles for $x = 0$, triangles for $x = 0.1$ and squares for $x = 0.2$.

is Boltzmann's constant, e is the electron's charge and α is a sample-dependent constant. By fitting the experimental data to these equations, I obtain the activation energies $E_{\rm hop}$ and E_S, respectively. The values of $E_{\rm hop}$ are also summarized in table 2. It is difficult to obtain an exact value of E_S because S is nearly constant at $T > T_c$; however, E_S could be estimated as about 5 meV for every compound. It is clear that the activation energy for conductivity, $E_{\rm hop}$, is much larger than the thermopower, E_S, as was reported before and has been considered as evidence of small-polaronic motion [26, 27]. A lot of recent experimental results, including transport measurements [28] and results obtained by microscopic techniques [14, 29] and from the isotopic effect [30], have given strong evidence that the polaron existing in the paramagnetic phase is of JT type. Therefore, it is considered that the JT distortion is the origin of the polaron above T_c in this system, too.

3.2. XPS measurement

In order to obtain information on the electronic structures, XPS measurement was carried out. Figure 5(a) illustrates the Mn 2p core-level XPS spectra of the $x = 0$ (A) and 0.2 (B) compounds at 133 K. The spectra display $2p_{3/2}$ and $2p_{1/2}$ peaks located around 642 and 654 eV binding energy, respectively. The most striking feature in this figure is the difference spectrum (C) for the $x = 0$ and 0.2 compounds, which is obtained by subtracting spectrum (A) from spectrum (B). This difference of the spectra indicates that the Mn $2p_{3/2}$ and $2p_{1/2}$ core levels shift to the higher-binding-energy side upon Ba doping.

In figure 5(b), the Mn 2p core-level XPS spectra for the $x = 0.2$ compound are shown. In this illustration, (A) and (B) indicate the results measured at room temperature and 133 K, respectively, and (C) is the difference spectrum: (C) = (B) − (A). There is no large difference in the XPS spectra between room temperature and 133 K. This result suggests that the electronic

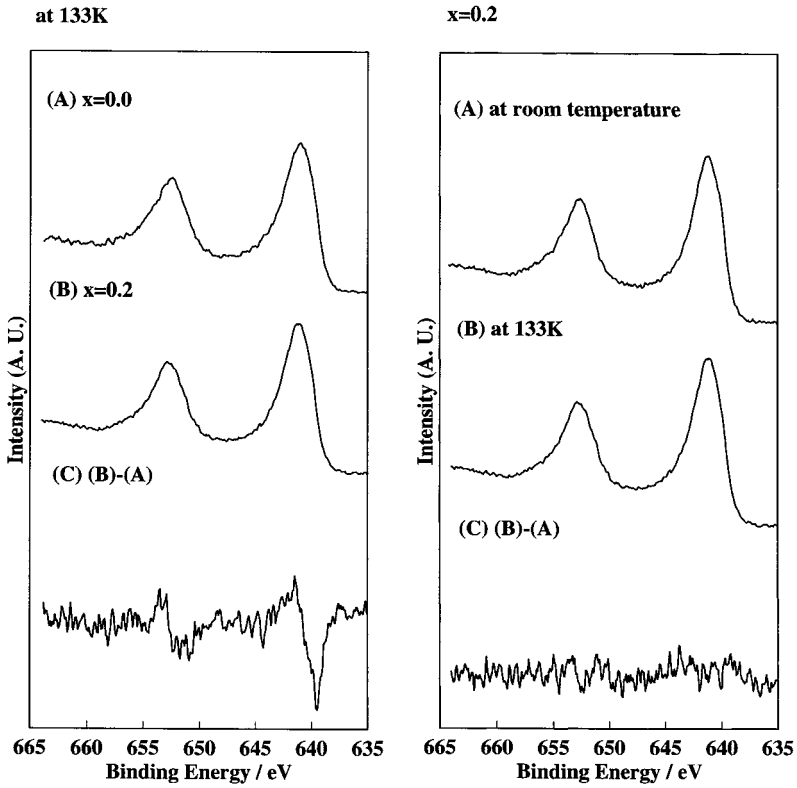

Figure 5. (a) Mn 2p XPS spectra for $x = 0$ (A) and $x = 0.2$ (B), and the difference spectrum (C) for the $x = 0$ and 0.2 compounds at 133 K. (b) Mn 2p XPS spectra at room temperature (A) and 133 K (B), and the difference spectrum (C) for the room temperature and 133 K spectra of the $x = 0.2$ compound.

structure is almost unchanged in the $x = 0.2$ compound even if temperature is lowered to 133 K from room temperature. As discussed above, the transport property at room temperature is dominated by the JT-type small polaron. Therefore, it is considered that in the $x = 0.2$ compound the JT distortion is present at temperatures at which the FM behaviour is observed, such as 133 K. It is suggested that there is a close relationship between the existence of the JT distortion at 133 K in the $x = 0.2$ compound and the shift of the Mn $2p_{3/2}$ and $2p_{1/2}$ core levels with Ba doping. The existence of the JT distortion at 133 K suggests that there is an insulator phase in the FM region in the $x = 0.2$ compound. It is highly probable that the replacement of Ca with Ba causes the phase separation into the FMM and insulator phases at $T < T_c$.

3.3. Fitting of the thermopower data

When carriers of two different kinds are present, each with a well-defined Seebeck coefficient S and conductivity σ, the measured thermopower is given by

$$S = \frac{\sigma_1 S_1 + \sigma_2 S_2}{\sigma_1 + \sigma_2} \tag{3}$$

where 1 and 2 denote the ferromagnetic metal and the insulator phases, respectively [31]. The quantities in equation (3) are approximated by

$$\sigma_1 = \frac{1}{\rho_1} = \frac{1}{\rho_a + \rho_b T^{2.5}} \tag{4}$$

$$S_1 \approx \frac{k_B}{e}\frac{\pi^2}{3}\frac{k_B T}{E_F} \tag{5}$$

$$\sigma_2 = \frac{A}{T}\exp\left(-\frac{E_{hop}}{k_B T}\right) \tag{6}$$

$$S_2 = \frac{k_B}{e}\left(\frac{E_S}{k_B T}\right) + S_\infty. \tag{7}$$

The form $\rho_1 = \rho_a + \rho_b T^{2.5}$ in equation (4) is used by Schiffer *et al* to fit empirically to the resistivity data for the FMM region observed in $La_{0.75}Ca_{0.25}MnO_3$ [32]. Here ρ_a is the resistivity due to the domain boundaries and other temperature-independent scattering mechanisms, and the $\rho_b T^{2.5}$ term represents a combination of electron–electron, electron–phonon and electron–magnon scattering. In a degenerate metal, the Seebeck coefficient is proportional to the first power of temperature and is given by the expression (5), in which E_F is the Fermi energy [31]. S_∞ in equation (7) is the Seebeck coefficient at asymptotically high temperatures—a measure of the entropy of crystalline and magnetic disorder. In the present study, two kinds, model A and B, of fitting are performed. In model A, the data are fitted over the entire temperature range for which the thermopower was measured. In this case, it is assumed that the phase separation occurs not only below T_c but also above T_c. This assumption leads to the suggestion that there is a ferromagnetic cluster in the paramagnetic region. The existence of a ferromagnetic cluster above T_c has been reported [33] and, to investigate this, the model A fitting is carried out. In model B, the thermopower data are fitted below T_c. In this model, it is assumed that the coexistence of the two phases is observed only below T_c.

A fit of equation (3) to the thermopower data on the $x = 0.2$ compound in which the phase separation is clearly observed is shown in figure 6. The open squares are the measured data, and the dashed and solid lines are the fits to the data using models A and B, respectively. As shown in figure 6, good fits with each model are obtained, and the parameters used for the fittings are summarized in table 3. It is necessary to confirm the relevance of the parameters obtained. A, E_{hop}, E_S and S_∞, which are the experimental data obtained here above T_c, are $5 \times 10^5\ \Omega^{-1}\ cm^{-1}$ K, 106 meV, 5 meV and $-33.3\ \mu V\ K^{-1}$, respectively. Comparing the fitting parameters of models A and B with the measured data, A and E_{hop} for model A are much larger and E_S smaller. A for model B is nearly equal to the experimental result, but E_{hop} is larger. This is explained as follows. In the small-polaron model, E_{hop} is normally assumed to be the sum of two relevant parameters, $E_{hop} = W_H + E_S$ [28, 34]. W_H is an activation energy and corresponds to the minimum energy that will achieve equivalence of the two neighbouring sites involved in the polaron hopping. From this equation, one can straightforwardly calculate W_H, and the values of the model B fitting and the experimental data are 126 and 101 meV, respectively. It is suggested that A, E_{hop} and E_S for the model B fitting are appropriate parameters to compare with the measured data which are obtained at $T > T_c$.

It is impossible to obtain the parameters for the FMM phase directly from the measured resistivity data, because these results reflect the competition between the FMM and insulator phases. Therefore, to confirm the relevance of the parameters ρ_a and ρ_b, the parameters obtained for each model are compared to the experimental result for $La_{0.75}Ca_{0.25}MnO_3$ which

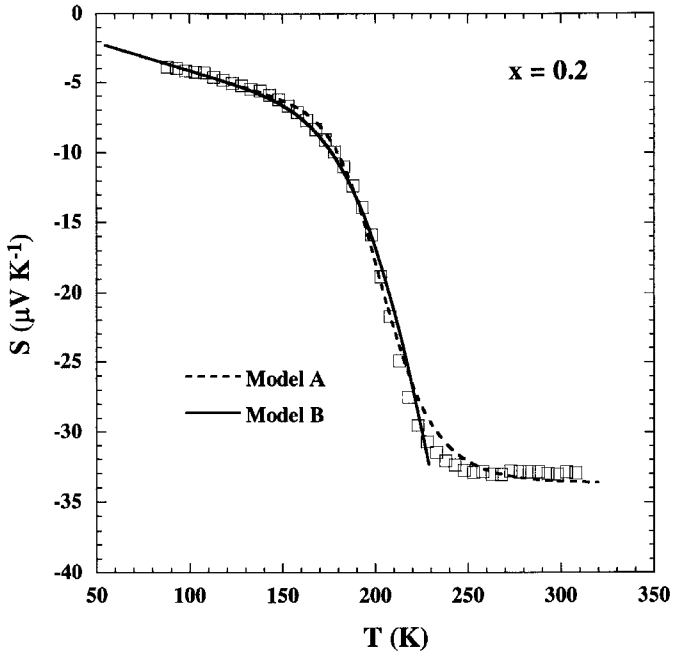

Figure 6. A fit of equation (3) to the thermopower data for $La_{0.5}Ca_{0.3}Ba_{0.2}MnO_3$. Open squares are the measured data, and the dashed and solid lines are the fits to the data with model A and B, respectively.

Table 3. Parameters used in equation (3) to fit the thermopower data for the $La_{0.5}Ca_{0.3}Ba_{0.2}MnO_3$ compound using models A and B.

Model	A (Ω^{-1} cm^{-1} K)	E_{hop} (meV)	E_S (meV)	S_∞ (μV K^{-1})	ρ_a (Ω cm)	ρ_b (Ω cm K$^{-2.5}$)
A	4.5×10^6	238	0.07	−33.5	1.0×10^{-3}	4.6×10^{-5}
B	4.5×10^5	146	20	−33.3	1.0×10^{-3}	2.7×10^{-7}

is reported by Schiffer *et al* [32]. In their study, ρ_a and ρ_b obtained from fitting to the resistivity data are about 1.7×10^{-3} Ω cm and 1.3×10^{-8} Ω cm K$^{-2.5}$, respectively. Comparing the fitting parameters for models A and B with these values, ρ_a from this study is nearly consistent with the previous one. The values of ρ_b for both models are larger, but the parameter for model B is near in order of magnitude. This indicates that the parameters of model B are practical values. It is probably impossible for the properties of the two phases to be exactly characterized by model B parameters. However, it is suggested that all of the parameters used for the model B fitting are physically acceptable values. This result is evidence that the phase separation takes place below T_c in the $x = 0.2$ compound.

4. Conclusions

So as to investigate the relation between electronic transport and magnetic properties and the lattice distortion in the Mn–O_6 octahedral network, I substitute Ba for Ca in $La_{0.5}Ca_{0.5-x}Ba_xMnO_3$ while keeping the fraction of Mn^{4+} at 0.48. Three sorts of compound ($x = 0$, 0.1 and 0.2) have been prepared and the four-probe dc resistivity, magnetic

susceptibility, thermopower and XPS were measured. Each compound exhibits a metal–insulator transition at T_{MI} and a magnetic transition at T_c, which is not the same as T_{MI}, and ferromagnetic insulator behaviour is observed for T in the range $T_{MI} < T < T_c$.

To quantify the lattice distortion in the Mn–O_6 octahedral network, the tolerance factor t and σ^2 are used. t and σ^2 both increase with x. Increasing t results in enhancement of the e_g-electron hopping between Mn^{3+} and Mn^{4+}. On the other hand, increase of σ^2 promotes the localization of e_g electrons. It is difficult to find an explanation of the results by considering just one effect. However, the coexistence of two competing effects accounts for the observed behaviours, and it is speculated that the phase separation into the FMM and insulator phases is caused by Ba doping below T_c.

A shift of the Mn 2p core level to the higher-binding-energy side on Ba doping is observed by XPS measurement at 133 K. On the other hand, there is no large change of the electronic structure between room temperature and 133 K for the $x = 0.2$ compound. These results suggest that the insulator phase exists at the temperature at which ferromagnetism is observed.

I find that a good fit of the thermopower data for the $x = 0.2$ compound is obtained by taking into account both the FMM and insulator phase contributions below T_c. It is suggested that the local lattice distortion created by Ba doping causes the phase separation at $T < T_c$, and it is considered that the complex behaviours observed in the resistivity and magnetic susceptibility measurements are affected by the competition between the two phases.

Acknowledgments

The chemical analyses were carried out by J Noro, and the XPS measurements by Y Shichi and Y Misono.

References

[1] Jin S, Tiefel T H, McCormack M, Fastnacht R A, Ramesh R and Chen L H 1994 *Science* **264** 413
[2] Gong G Q, Canedy C L, Xiao Gang, Sun J Z, Gupta A and Gallagher W J 1995 *Appl. Phys. Lett.* **67** 1783
[3] Tomioka Y, Asamitsu A, Moritomo Y, Kuwahara H and Tokura Y 1995 *Phys. Rev. Lett.* **74** 5108
[4] Zener C 1951 *Phys. Rev.* **82** 403
[5] Millis A J, Littlewood P B and Shraiman B I 1995 *Phys. Rev. Lett.* **74** 5144
[6] Millis A J, Shraiman B I and Mueller R 1996 *Phys. Rev. Lett.* **77** 175
[7] Mahesh R, Mahendiran R, Raychaudhuri A K and Rao C N R 1995 *J. Solid State Chem.* **120** 204
[8] Radaelli P G, Marezio M, Hwang H Y and Cheong S-W 1996 *J. Solid State Chem.* **122** 444
[9] Hwang H Y, Cheong S-W, Radaelli P G, Marezio M and Batlogg B 1995 *Phys. Rev. Lett.* **75** 914
[10] Rodriguez-Martinez L M and Attfield J P 1996 *Phys. Rev.* B **54** R15 622
[11] Maignan A, Martin C, van Tendeloo G, Hervieu M and Raveau 1999 *Phys. Rev.* B **60** 15 214
[12] Terai T, Kakeshita T, Fukuda T, Saburi T, Takamoto N, Kindo K and Honda M 1998 *Phys. Rev.* B **58** 14 908
[13] Allodi G, De Renzi R, Guidi G, Licci F and Pieper M W 1997 *Phys. Rev.* B **56** 6036
[14] Lanzara A, Saini N L, Brunelli M, Natali F, Bianconi A, Radaelli P G and Cheong S-W 1998 *Phys. Rev. Lett.* **81** 878
[15] Mori S, Chan C H and Cheong S-W 1998 *Phys. Rev. Lett.* **81** 3972
[16] Huang Q, Lynn J W, Erwin R W, Santoro A, Dender D C, Smolyaninova V N, Ghosh K and Greene R L 2000 *Phys. Rev.* B **61** 8895
[17] Ramirez A P, Schiffer P, Cheong S-W, Chen C H, Bao W, Palstra T T M, Gammel P L, Bishop D J and Zegarski B 1996 *Phys. Rev. Lett.* **76** 3188
[18] Roy M, Mitchell J F, Ramirez A P and Schiffer P 1999 *J. Phys.: Condens. Matter* **11** 4843
[19] De Teresa J M, Ibarra M R, García J, Blasco J, Ritter C, Algarabel P A, Marquina C and del Moral A 1996 *Phys. Rev. Lett.* **76** 3392
[20] Guitiérrez J, Peña A, Barandiarán J M, Pizarro J L, Hernández T, Lezama L, Insausti M and Rojo T 2000 *Phys. Rev.* B **61** 9028
[21] Shannon R D 1976 *Acta Crystallogr.* A **32** 751

[22] Anderson P W and Hasegawa H 1955 *Phys. Rev.* **100** 675
[23] Rodriguez-Martinez L M and Attfield J P 1998 *Phys. Rev.* B **58** 2426
[24] Hundley M F and Neumeier J J 1997 *Phys. Rev.* B **55** 11 511
[25] Emin D and Holstein T 1969 *Ann. Phys., NY* **53** 439
[26] Jamie M, Hardner H T, Salamon M B, Rubinstein M, Dorsey P and Emin D 1997 *Phys. Rev. Lett.* **78** 951
[27] Mott N F 1993 *Conduction in Non-Crystalline Materials* (New York: Oxford University Press)
[28] De Teresa J M, Dörr K, Müller K H, Schultz L and Chakalova R I 1998 *Phys. Rev.* B **58** R5928
[29] Louca D, Egami T, Brosha E L, Röder H and Bishop A R 1997 *Phys. Rev.* B **56** R8475
[30] Zhao Guo-meng, Conder K, Keller H and Müller K A 1996 *Nature* **381** 676
[31] Rubinstein M, Gillespie D J, Snyder J E and Tritt T M 1997 *Phys. Rev.* B **56** 5412
[32] Schiffer P, Ramirez A P, Bao W and Cheong S-W 1995 *Phys. Rev. Lett.* **75** 3336
[33] De Teresa J M, Ibarra M R, Algarabel P A, Ritter C, Marquina C, Blasco J, García J, del Moral A and Arnold Z 1997 *Nature* **386** 256
[34] Jaime M, Salamon M B, Rubinstein M, Treece R E, Horwitz J S and Chrisey D B 1996 *Phys. Rev.* B **54** 11 914